INDUSTRIAL AND CIVIL ENGINEERING AND ECONOMICS

DOI 10.15826/rjcst.2017.1.001 УДК 624.5

Lo Presti D. [1], *Angina A.* [2], *Steri A.* [3]
[1–3] University of Piza,
Piza, Italy

E-mail: [1]*diego.lopresti@dic.unipi.it*

FINAL DESIGN OF THE ONE-SPAN SUSPENSION BRIDGE FOR THE MESSINA STRAIT CROSSING: SOME GEOTECHNICAL ISSUES

Abstract. The authors briefly summarise the recent history of the final design of the one-span suspension bridge for the Messina strait crossing. The general features of the structure, the geological and environmental site conditions and the main geotechnical design issues are described referring to previous publications. Details concerning some specially-devised in situ and laboratory tests are also reported.

Keywords: one-span suspension bridge, Messina strait crossing, structure, geological, environmental, site conditions, tests.

Ло Прести Д. [1], *Ангина А.* [2], *Стери А.* [3]
[1–3] Университет Пизы,
Пиза, Италия

E-mail: [1]*diego.lopresti@dic.unipi.it*

ОКОНЧАТЕЛЬНЫЙ ПРОЕКТ ОДНОПРОЛЕТНОГО ВИСЯЧЕГО МОСТА ЧЕРЕЗ ПРОЛИВ МЕССИНА: НЕКОТОРЫЕ ГЕОТЕХНИЧЕСКИЕ АСПЕКТЫ

Аннотация. В статье кратко описана история разработки окончательного проекта однопролетного висячего моста через пролив Мессина. Основные особенности конструкции, геологические и экологические условия площадки строительства и основные особенности геотехнического проекта описаны на основе предыдущих публикаций. Описаны особенности проведенных экспериментальных и лабораторных исследований.

Ключевые слова: однопролетный висячий мост, пролив Мессина, конструкция, геологические и экологические условия, площадка строительства, испытания.

1. Recent history of the bridge

The Italian territory consists of mainland, with a typical boot shape, two great islands (Sardinia of 24,000 km^2 and 1.3 million inhabitants; Sicily of 26,000 km^2 and 4.9 million inhabitants), and several small islands disseminated in the Mediterranean Sea (Fig. 1).

Several solutions have been studied for the Messina Strait crossing to connect Sicily to the mainland. The first attempt was probably done by the old Romans who constructed, at the time of the first war against Carthage, a temporary pontoo-bridge to allow an army to pass from the mainland to Sicily.

Fig. 1. Location of the bridge crossing

More recently, other solutions have been considered (underground tunnel, submerged tunnel, two span suspension bridge, one span suspension bridge). It is worth nothing, that all these solutions guarantee the navigation. Moreover, the construction site is characterized by a very high seismicity and extremely hostile both atmospheric and marine conditions. The submerged tunnel was considered unfeasible because of the very strong sea currents. For the same reason the two span suspension bridge was considered unfeasible. The considerable depth of the sea floor was also a reason to exclude these solutions. The underground tunnel was considered unfeasible for the presence of active faults and for logistic reasons. In fact the two entrance points should have been located at tens of kilometers far from the two main cities (Messina and Reggio Calabria), thus excluding local traffic. Since 1981, the "Stretto di Messina Spa (SdM)" was established for accomplishing the final design of the bridge and for its future construction and maintenance. The preliminary design of the one span suspension bridge was ready on 2005. On October 2005 Eurolink Spa (leaded by Impregilo Spa) won the international bid offering 3.88 billion euros. On 20 December 2009, the general contractor, Eurolink, completed the final design which was approved by the contracting SdM and the National Authorities for railways (FFSS) and roads (Anas). Due to the subsequent economical crisis, an additional agreement between SdM (contracting) and Eurolink (genera contractor) was requested by the Italian Parliament. Such an agreement was not signed before the deadline, fixed to the 1st March 2013, and any activity was therefore stopped. On 27 September 2016 the Italian Prime Minister, Matteo Renzi, announced the intention to proceed with the bridge construction, confirming the interest of Chinese investors.

2. Geological, Geotechnical and Environmental Conditions

The subsoil conditions on both sides of the Messina Strait consist of gravelly deposits of Holocene and Pleistocene age underlain by soft rocks of Pliocene and Miocene Epochs. The present section summarizes the geotechnical characterization of the sand and gravel deposits, in connection with the design of the one span suspension bridge over the Messina Strait. Crova et al. 1992 and Jamiokowski and Lo Presti (2003) have already dealt with the same topic. Extensive geological and geotechnical investigations were undertaken in the period 1984–1992. A specific geological investigation has been undertaken for the area of interest (Sitec 1985) and the related activities are summarized in Table 1. The geotechnical investigation for the preliminary design of the one span suspension bridge consisted of the activities summarized in Table 2.

Mainly geotechnical boreholes and in situ tests have been carried out, although some laboratory tests on reconstituted samples and the evaluation of index properties in the laboratory have also been performed (Ismes 1985, Ferrante 1988).

The geology of the area of interest has been defined by the specific investigations previously mentioned (Sitec 1985) and by literature data (Atzori et al. 1983).

These investigations were mainly aimed at defining stratigraphy, geological structure, geo-morphology, with special attention being paid to fault activity and fault throw.

Table 1

Geological investigation

Type of investigation	Notes
Geological survey (scale 1:10.000)	Investigated area: 250 km^2
Structural geological survey of faults	–
Rotary borings with continuum coring, performed on both Calabrian and Sicilian shores	Depth from 10 to 140 m. Totally 22 boreholes were performed and 1500 m of soil were cored
Micro-paleontologic analyses	112 shallow samples
Mineralogic analyses	86 samples
Radio-carbon dating	10 samples
Gamma-logging	13 boreholes
Investigation trenches	Three different locations

Table 2

Soil investigation program

Type of test	Calabria		Sicily	
	Foundation	Anchor	Foundation	Anchor
BH (1)	4	5	2	3
SPT (2)	7	6	7	6
LPT (2)	5	5	5	5
PLT (3)	None	3	None	3
Pumping test	1	None	1	None
CPT	1	None	3	None
CH (4)	2	2	2	1
SASW	1	1	1	3
RCT (5)	5	None	9	None
RCT (6)	None	None	22	None
CTX (7)	16	None	17	None

BH = boring with samples; SPT = standard penetration test; LPT = large penetration test; PLT = plate load test; CPT = static one penetration test; CH = cross hole method; SASW = special analyses of surfaces waves; RCT resonant column test; CTX = undrained and drained cyclic triaxial tests

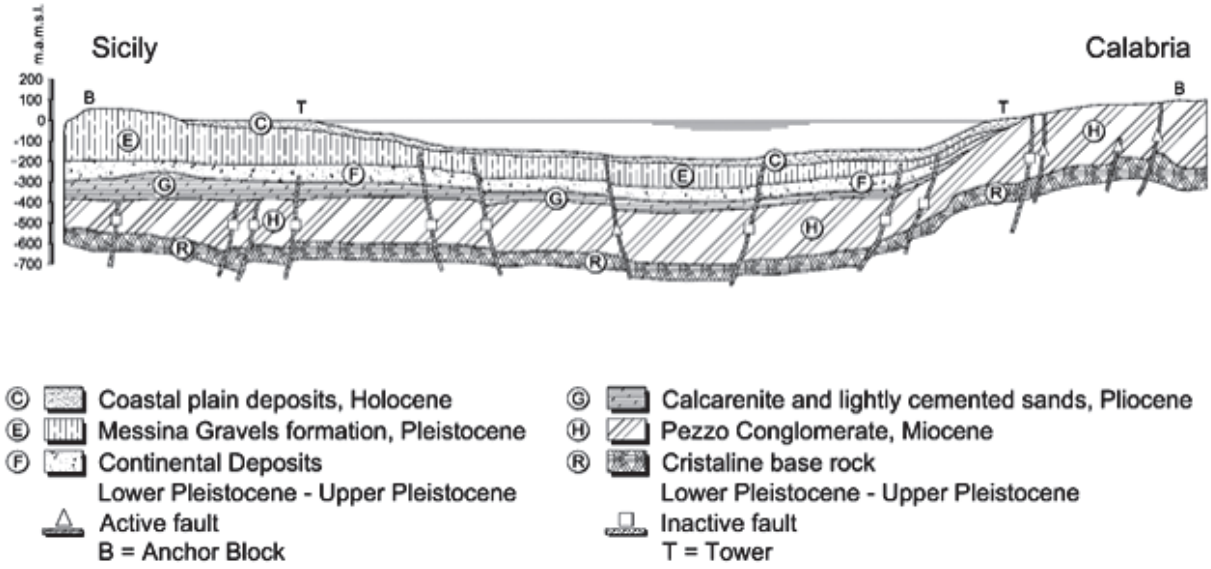

Fig. 2. Semplified geological cross section

Fig. 2 shows the simplified geological cross section along the bridge axis. The Figure also shows the location of faults that have been active since the lower Pliocene.

It is possible to observe a graben-like structure with several normal faults having an average inclination between 60° and 80°. The main faults of the region can be grouped in four systems with different strike: a) NE-SW, b) N-S, c) E-W, d) NW-SE. The first one (NE-SW) seems to play a major role. Although there is no evidence of normal faults cutting the uppermost Holocene sediments, several of them are supposed to be geologically active (Sitec 1985, Faccioli 1994). The most severe fault throw, for the bridge under design, has been evaluated to be about a few tens of cm for the 2000 year event and it has been shown that this would not cause undue deformations in the tower foundations and structure (Faccioli 1994).

The shallow granular deposits are from Pleistocene (Messina Gravel Formation — MGF) and Holocene (Coastal Plain Deposits — CPD).

The MGF consists mainly of gravels and pebbles in a rich sand matrix, often well graded, having a mean grain size (D_{50}) of about 10 mm and a maximum grain size (D_{max}) of about 80 to 100 mm. Gravel grains are rounded or flat. Interbedded lenses of sand and of quartz-mudstone are repeatedly encountered.

Sometimes, gravels are $CaCO_3$ cemented with remains of shells. Strata are from 0.5 to 1.0 m thick, inclined at about 35° to 45° towards the axis of the Messina Strait. Deposition environment was deltaic-littoral. Thickness is from few meters to about 300–400 meters. The age of deposits is medium Pleistocene, as testified by the discovery of ancient fossils of elephants (Elephas antiquus; see Bonfiglio and Berdar 1979). No sign of paleo liquefaction has been observed.

The CPD formation is a sequence of sandy — gravelly layers with the occasional occurrence of brown — blackish thin lenses and layers rich in organic matter. The thickness ranges from 5 to 70 m in the Calabrian shore. The thickness of this formation in the Sicilian shore is not certain because of the absence of micro paleontological remains and the similarity, from a lithological point of view, between MGF and CPD. Sediment genesis is related to the repeated oscillation of the sea level. The sedimentation environment is coastal marine with episodes of continental sedimentation. Radio carbon dating gives a maximum age of 17.000 years. Signs of paleo liquefaction have been observed (Sitec 1985). Liquefaction phoenomena were caused by the 1908 Messina Earthquake ($M_w = 7.2$).

Fig. 3 shows a cross section of the subsoil conditions on the Sicilian shore.

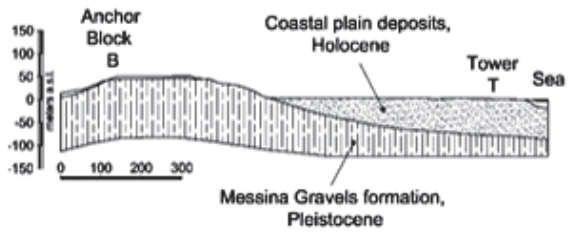

Fig. 3. Soil profile on Sicily shore

As far as the location of the anchor block is concerned, from the ground surface down to the maximum explored depth of 100 m, see Fig. 4, the soil consists of sand and gravel of medium Pleistocene age (MGF), which, based on geological borings and geophysical investigations, extend to a depth of at least 180 m below ground level.

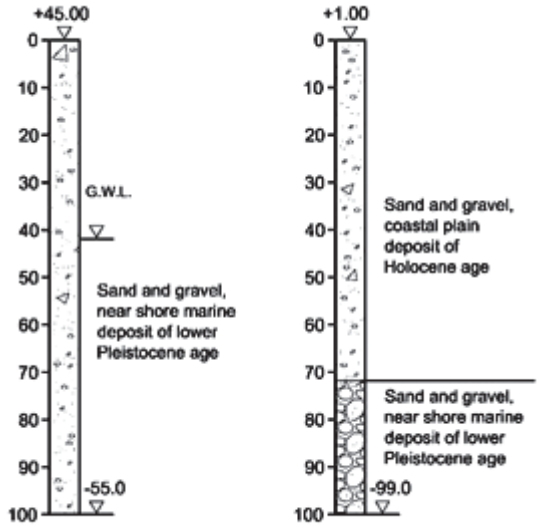

Fig. 4. Soil profile Sicilian shore

Under the bridge tower, the upper part of the subsoil profile consists of sand and gravel of Holocene age (CPD) having a thickness of 70 m. As far as the Calabrian anchor is concerned, Pezzo conglomerate extends from ground level down to 300 m. The soil profile below the bridge tower on Calabrian shore is shown in Fig. 5.

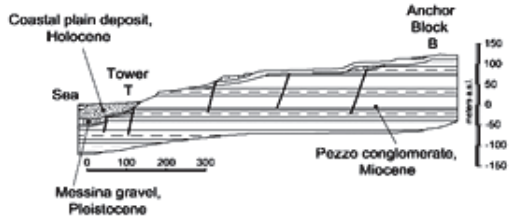

Fig. 5. Soil profile on Calabrian shore

It is possible to notice that the upper part of the soil consists of CPD having a thickness of about 25 to 30 m, overlying the MGF layer, which extends to a depth of about 45 m.

Ground water level coincides with the mean sea level so that at both tower foundations (Sicilian and Calabrian shores) the water table is located no more than 2.0 m below the ground level. At the anchor block location on the Sicilian shore the water table is about 43.0 m below the ground level, while as far as the anchor block location on the Calabrian shore is concerned, the water table is on average about 8 m below the ground level, i. e. about 100 m above m. s.l.

Figs. 6 to 9 show the grain size distributions of CPD and MGF as inferred from the soil samples obtained from geotechnical boreholes (BH) using a sampler having internal diameter ID = 100 mm, from Large Penetration Tests LPT's (ID = 100 mm) and Standard Penetration Tests SPT's (ID = 35 mm). Larger soil samples have been obtained from wells excavated for the execution of Plate Load.

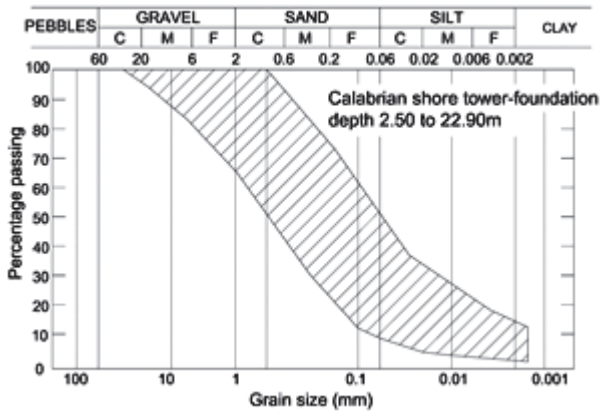

Fig. 6. Graduation curves of MGF (Sicilian shore)

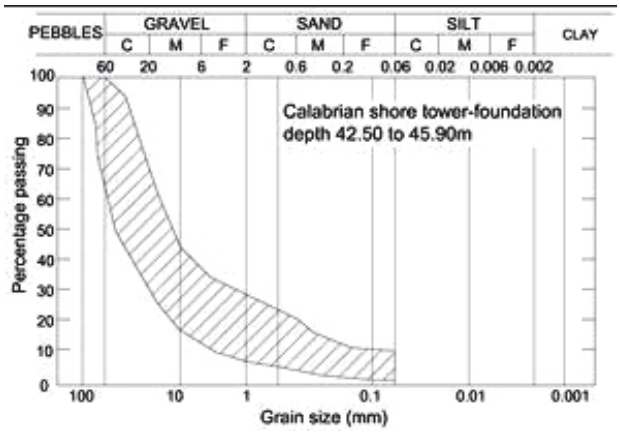

Fig. 7. Gradiation curves of CPD (Sicilian shore)

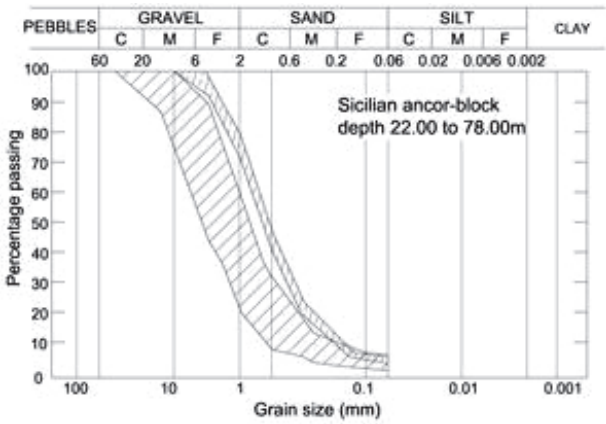

Fig. 8. Gradiation curves of CPD (Calabrian shore)

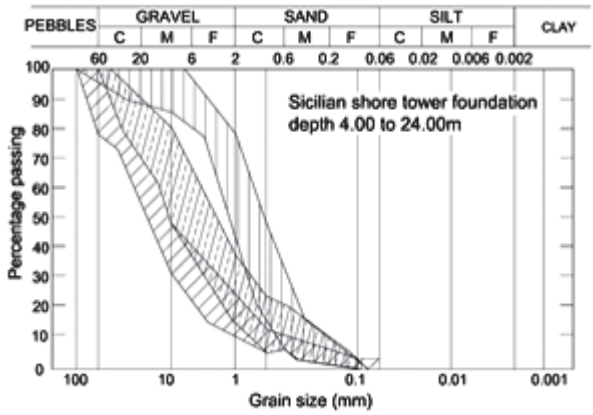

Fig. 9. Gradiation curves of MGF (Calabrian shore)

Relative density (D_r) has been inferred from penetration test results:

- N_{SPT}, i.e. the number of blows for a 30 cm penetration, measured during Standard Penetration Tests (SPT);
- N_{LPT}, i.e. the number of blows for a 30 cm penetration, measured during Large Penetration Tests (LPT).

SPTs were carried out using a hardened-steel spoon sampler with ID = 34.9 mm and OD = 50.8 mm, similar to that suggested by the ISSMGE reference test procedure (Decourt et al. 1988). The SPT sampler was driven into the soil using rods having ID = 36 mm and OD = 50 mm. The LPT equipment was specifically developed for the Messina Strait site in order to investigate the possible influence of gravel particles on the measured blow/count. The hardened-steel sampler (Fig. 10) was used as a penetration tool. It has ID = 115 mm and OD = 140 mm and contains a plastic liner 5 mm thick. It is driven into the soil using rods having ID = 100mm and OD = 133mm.

The LPT sampler is driven 450 mm into the soil from the bottom of a borehole, counting the number of blows necessary for penetrating every 150 mm.

Table 3 summarizes the characteristics of the above described LPT and, for comparison, those of other Large Penetration Tests used in North America (Harder and Seed 1986, Harder 1988, Sy et al. 1995) and in Japan (Kaito et al. 1971, Yoshida 1988, Yoshida et al. 1988).

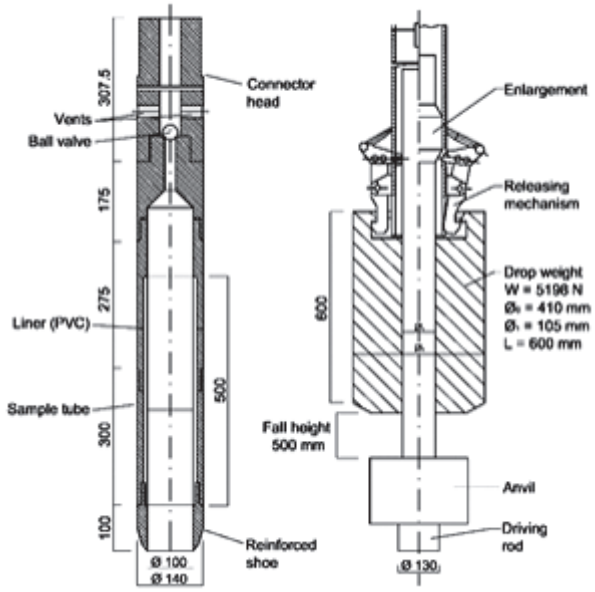

Fig. 10. LPT sampler

Both SPT and LPT were carried out in cased boreholes having a diameter of 75 and 200 mm respectively. The boreholes were always filled with bentonite mud for the purpose of preventing hydraulic inflow and consequent loosening of the soil at the bottom of the hole The energy delivered to the driving rod was measured during both SPT and LPT by means of a load cell consisting of 1 meter long rod segment, instrumented with strain gauges (Schmertmann and Palacios 1979). Capacity and accuracy of such a load cell were 150 kN and 2% respectively. In the case of the LPT, an accelerometer with a range of 0 to 5000g was also used. Both instruments (load cell and accelerometer) were placed just beneath the anvil. Measurements of the energy delivered to the driving rods enabled us to compute the energy ratio ER (%), which indicate the percentage of the impact energy effectively transmitted to the sampler. The energy measurements were performed for depths between 10 and 50 m below the ground level.

In order to calibrate the LPT and compare its results with those of SPT, preliminary tests were performed at the S. Prospero site in the well documented Po river sand

Table 3

Characteristics of dynamic penetration tests

	Standard penetration test	Large penetration test (1)	Large penetration test (2)	Large penetration test (3)
Drive method	Fall weight	Fall weight	Fall weight	Diesel hammer
Weight	623 N	981 N	5592 N	—
Drop height	760 mm	1500 mm	500 mm	—
Impact energy	473 Nm	1472 Nm	2796 Nm	344–6512 Nm
Drive length sampler	450 mm	450 mm	450 mm	300 mm
OD	51 mm	73 mm	140 mm	165 mm
ID	35 mm	50 mm	100 mm	Closed end

(Baldi et al. 1988, Baldi et al. 1989a, 1989b, Jamiokowski and o Presti 2003). Examples of the statistical distribution of measured ER in CPD and MGF are shown in Figs. 11 and 12.

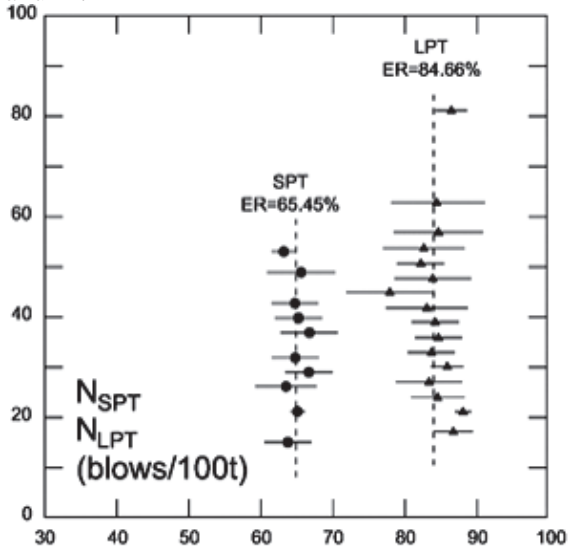

Fig. 11. SPT and LPT rod energy ratio Messina strait Holocene sand and gravel

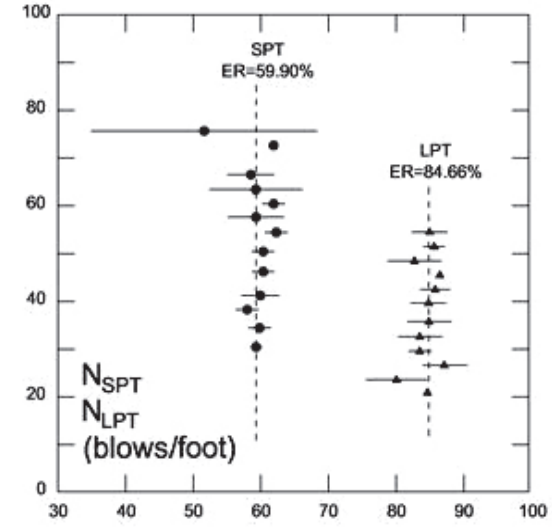

Fig. 12. LPT rod energy ratio Messina strait Pleistocene sand and gravel

Table 4 summarizes the obtained values of ER and N_1 (60). The last is the penetration resistance normalised to the ER = 60 % and to the value of the effective overburden stress σ'_{vo} = 98.1 kPa. Normalization with respect to the ER is made according to Schmertmann and Palacios (1979) and Skempton (1986). The following equation is used:

$$N_{60} = N_{SPT} \cdot \frac{ER}{60} \quad (1)$$

Normalization with respect to the overburden stress has been done according to Liao and Whitman (1985) using the following equations:

$$(N_1)_{60} = N_{60} \cdot C_N \quad (2)$$

$$C_N = \left(\frac{p_a}{\sigma'_{vo}} \right)^{1/2} \quad (3)$$

where: p_a = 98.1 kPa; σ'_{vo} = vertical effective geostatic stress.

In Fig. 13 is shown the ratio $|N_{1\,(60)}|_{SPT}/|N_{1\,(60)}|_{LPT}$, as a function of mean grain size.

This ratio is, on average, close to 1.0, i. e. the capability of LPT is close to that of the SPT as shown in the recent work by Daniel (2000). This is true despite the increased driving energy and efficiency of the LPT driving system, because the delivered energy is necessary to overcome the base resistance and the shaft friction (Schmertmann 1979), which of course increase with the sampler sizes. It is also worthwhile to notice that the aforementioned ratio decreases as the mean grain size increases. Kokusho (1988) commented on such a trend through the following considerations:

- the N_{SPT} / N_{LPT} ratio is strongly dependent on energy intensity ratio which is the ratio of energy intensity between SPT and LPT;
- energy intensity is defined as (Impact energy)/Area;
- energy intensity ratio for penetration with open end [Area= $\pi/4$ ($OD^2 - ID^2$)] is 1.06, while it becomes equal to 0.87 for penetration with closed end [Area= $\pi/4$ $(OD)^2$];
- it is supposed that penetration occurs with closed end as the mean grain size increases. Therefore, the decrease of the energy intensity ratio explains the observed decrease in the N_{SPT} / N_{LPT} ratio.

Table 4

N_{SPT} vs N_{CPT} in granular deposits

Site	Deposit	$[N_{1\,(60)}]_{SPT}$				$[N_{1\,(60)}]_{CPT}$			
		ER ± St. dev	Mean ± St.dev	Norm.	Skew	ER ± St. dev	Mean ± St.dev	Norm.	Skew
San Prospero	Poriver sand	56 ± 3	20 ± 8	15	0.63	84 ± 3	18 ± 7	17	0.21
	Holocene sand and gravel (CPD)	66 ± 3	24 ± 10	16	0.85	85 ± 6	30 ± 12	26	0.42
Messina Strate	Pleistocene sand and gravel (MFG)	61 ± 3	27 ± 7	25	0.29	85 ± 6	29 ± 9	23	0.67

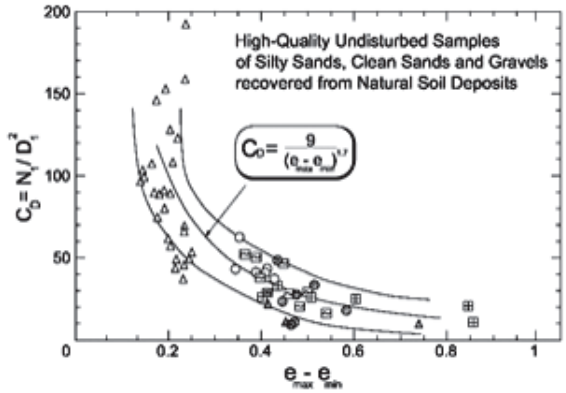

Fig. 13. $[N_1(60)]_{SPT}$ vs $[N_1(60)]_{LPT}$

The relative density has been obtained by means of the empirical relationships, reported below Cubrinovski and Ishihara (1999):

$$\frac{(N_1)_{78}}{D_R^2} = C_D \qquad (4)$$

$$C_D = \frac{9}{(e_{max} - e_{min})^{1.7}} \qquad (5)$$

Cubrinovski and Ishihara (1999) obtained such empirical correlations by considering the relative density of high quality undisturbed samples, mainly retrieved by means of in situ soil freezing at several Japanese sites where SPT or LPT have also been performed. Cubrinovski and Ishihara (1999) assume that for both SPT and LPT the equipment efficiency is 78 %, which is typical of the Japanese-SPT practice (Skempton 1986). Fig. 14 shows eq. (5) and the related empirical data, in order to appreciate the accuracy of such an equation.

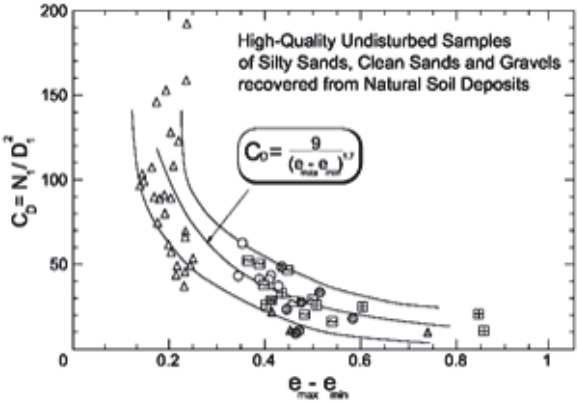

Fig. 14. Relationship between N_1/D_1^2 and void ratio range

For the case under consideration, the difference $(e_{max} - e_{min})$ has been inferred by D_{50}, using eq. (6):

$$e_{max} - e_{min} = 0.23 + 0.06/D_{50} \qquad (6)$$

The obtained values of D_R for CPD exhibit a decrease with depth. These values ranged in between 40 to 60 %. Similar values of D_R have been obtained in the MGF but without no tendency to decrease with depth. These results are shown in Fig. 15 and 16 where, for comparison, the values inferred according to the Gibbs and Holtz (1957) method are also shown.

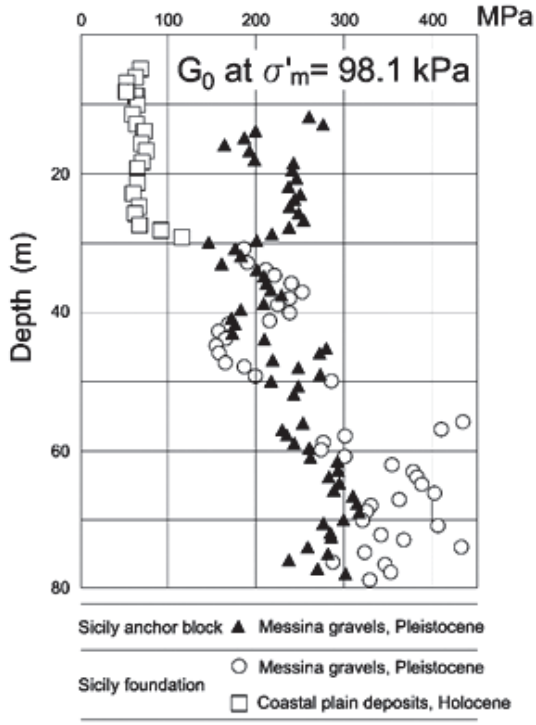

Fig. 15. Normalized strain shear modulus

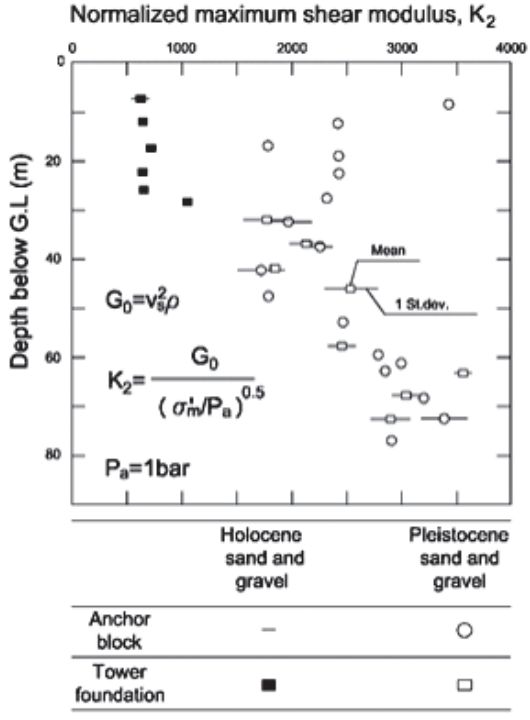

Fig. 16. Normalized shear modulus of sand and gravel from seismic tests

It is clear that, in the case of gravelly soils, the Gibbs and Holtz (1957) method overestimate the relative density and led to unreliable results. However, the main uncertainty, when using eqs. (4) and (5), is that the effective efficiency of the Japanese LPT has never been measured. Cross Hole (CH) tests and SASW tests (Nazarian and Stokoe 1983) have been used to measure the Shear wave velocity. Basically, the same shear wave velocities have been obtained from CH and SASW (Seismic Analyses of Surface Waves). Three boreholes extending up to 80 m below ground level have been used for each CH test, thus allowing one to use the "true visual interval method" for test interpretation. An electro-magnetic source, specialised in the generation of shear waves, with the possibility of polarity inversion, has been used. Vertical geophones were clamped at given depths by means of a pneumatic system.

The small strain shear modulus (G_c) and the modulus number K_2, as defined by Seed et al. (1985), has been obtained from the shear wave velocity measurements for both CPD and MGF. More specifically, K_2 is defined in the following way and represents the modulus dimensionless constant of eq. (7), equal to 1710, multiplied by the void ratio function:

$$G_o = 1710 \cdot (\sigma_c')^{0.54} \cdot p_a^{0.46} \cdot \frac{(1.32-e)^2}{(1+e)} \quad (7)$$

$$G_o = K_2 \cdot p_a^{1-n} \cdot (\sigma_m')^n \quad (8)$$

$$G_o = \rho \cdot V_s^2 \quad (9)$$

where: $\sigma'_m = (\sigma'_{vo} + 2\,\sigma'_{ho})/3$ is the mean effective stress; n is the modulus exponent, which depends on the coefficient of uniformity (Brignoli et al. 1991); in this case it was assumed equal to 0.5.

The modulus number, as obtained in the case of reconstituted samples of CPD from eq. (7) for relative densities of 50 to 60 %, ranges mainly from 800 to 900 and coincides with the modulus number obtained from in situ geophysical tests in CPD. The modulus number of MGF, as obtained from in situ tests results using eq. (8), is much greater than that of CPD (see Fig. 15). This Figure refers to a spot (Sicilian shore) where the contact between the two formations was located by geologists at a depth ranging from 36 to 38 m. The difference of G_c in Holocene and Pleistocene sand and gravel appears evident (see also Fig. 16). Based on the already indicated similarities between the two deposits, it is postulated that this difference should be attributed to their different age.

To understand the reasons for the differences in stiffness between CPD and MGF, a number of outcrops of MGF existing in the immediate surroundings of the construction site have been investigated (Bosi 1990), leading to the conclusion that within the Pleistocene sand and gravel formation:

- weak to occasionally strong bonding due to cementation (calcium carbonate and iron oxides), together with other signs of early diagenesis exist;
- no sign of liquefaction phenomena which might have occurred in the past were observed.

In contrast, an absence of cementation phenomena has been ascertained in Holocene sand and gravel based on the information collected from shallow excavations in CPD and from the examination of the cores of the borings. Considering that SPT and LPT results are essentially the same in CPD and MGF, it emerges that penetration tests which induce a large straining in the surrounding soil obliterate the effects of soil structure due to processes like aging, light cementation and other phenomena of early diagenesis as described by Dusseault and Morgenstern (1979), Mitchell (1986), Palmer and Barton (1987), Barton and Palmer (1989), Mesri et al. (1990) and Schmertmann (1991). In contrast, the above mentioned phenomena strongly influence soil stiffness at small strains. A complete characterization of the Messina granular deposits is reported in the paper by Jamiolkowski and Lo Presti (2003). This characterization includes info rmation on K_o, stiffness and drained/undrained strength parameters.

3. General Features and Main Geotechnical Design Issues

The main features of the bridge are listed below:

- length of the main span: 3300 m
- length of the two side spans: 183 m
- road traffic lanes: 2 (each consists of fast speed + normal speed + emergency lane)
- railway lines: 2 (each consists of track + service lane for tired vehicles)
- service sections: 2 independent lanes for service vehicles and pedestrians)
- height above the sea level: 65 m
- maximum traffic capacity: more than 200 trains per day; 4500 vehicles per hour in one direction

The deck cross section is shown in Fig. 17.

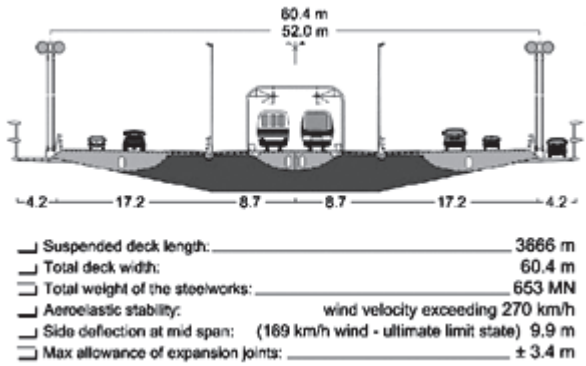

Fig. 17. Deck cross section

Fig. 18 shows a cross section along the bridge axis. It appears that the most relevant geotechnical design issues

are related to the tower foundations and anchor blocks.

The bridge was designed according to the Limit State approach by considering a 200 year service life and three levels of earthquake and actions. More specifically, return periods of 50, 400 and 2000 years were considered. Table 5 shows the actions for the three considered levels. The third level design earthquake (PGA = 058 g) represents the 1908 Messina earthquake (M_w = 7.2, XI MCS Epicentral Intensity, return period of 2000 years). It is worth noting that the estimated natural period of the bridge is of about T = 25s. Therefore, the most severe action is represented by the wind.

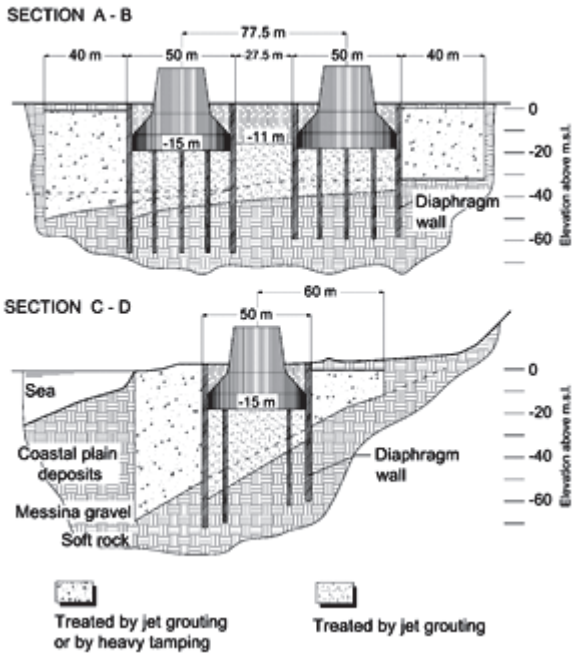

Fig. 18. Tower foundation on Calabrian shore

Tower foundations on both the Sicilian and Calabrian shores were designed in order to reach a depth of about 16 m below ground level (G.L), lying on the gravelly soils improved by intensive jet-grouting treatment.

Table 5

Messina Strait Crossing design earthquake and wind

	Peak ground acceleration (free field condition)	Wind velocity u (10)* (m/s)	Return periods (years)
1st level	0.08 g	36	50
2nd level	0.29 g	42	400
3rd level	0.58 g	46	2000
(*) at +10 m above m. s.l. $u(z) = u(10)(z/10)^{0.135}$ $u(z) = u(300)$		z = elevation above m. s.l. for 10 m < z < 300 m for z > 300 m	

The major problems for the design of Tower foundations may summarized as follows:

- dewatering of deep excavations located close to the shoreline (Sicilian and Calabrian shore);
- liquefaction during third level earthquake (Sicilian and Calabrian shore);
- non uniform soil support (Calabrian shore);
- seismic stability of adjacent steep underwater slope (Calabrian shore).

Fig. 19 shows the transversal and longitudinal sections of the foundations (Sicilian shore). The figure clarifies in a self evident way the last two points above mentioned.

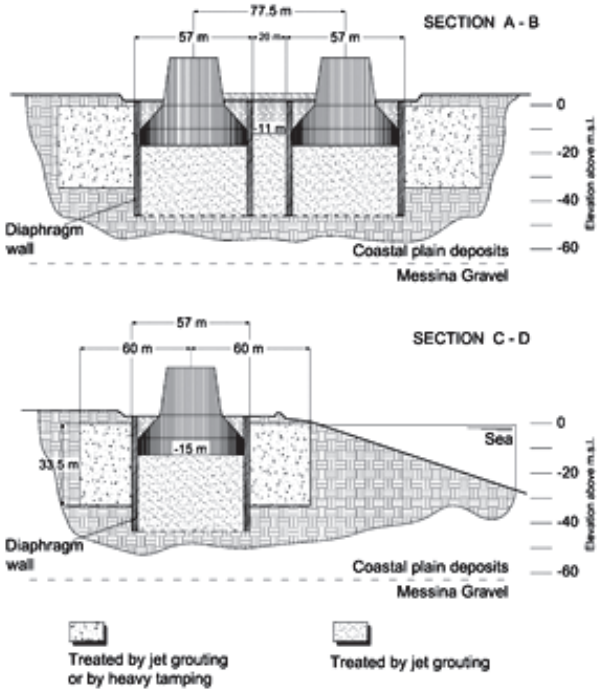

Fig. 19. Tower foundation on Sicilian shore

The intensive jet-grouting treatment was intended for construction purposes (dewatering) and also to mitigate the liquefaction risk. During third level earthquake, liquefaction could occur in CPD and MGF as well because the very high pressure induced in the soil by the towers.

Anchor blocks were designed in order to reach a depth of about 50 m.

The major problems for the design of Anchor blocks may be summarized as follows:

- adverse topography (Sicilian shore)
- temporary earth support of deep excavations (more than 50 m at Sicilian and Calabrian Shore)
- permanent displacements during earthquakes (Sicilian and Calabrian shore).

Figs. 20 and 21 shows a scheme of the Anchor blocks (Calabrian and Sicilian shore respectively).

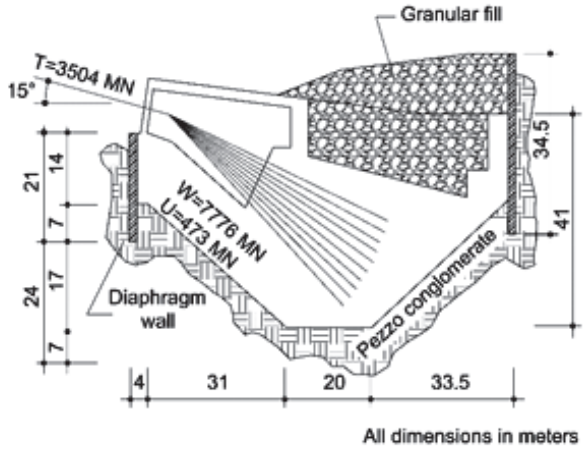

Fig. 20. Anchor block on Calabrian shore

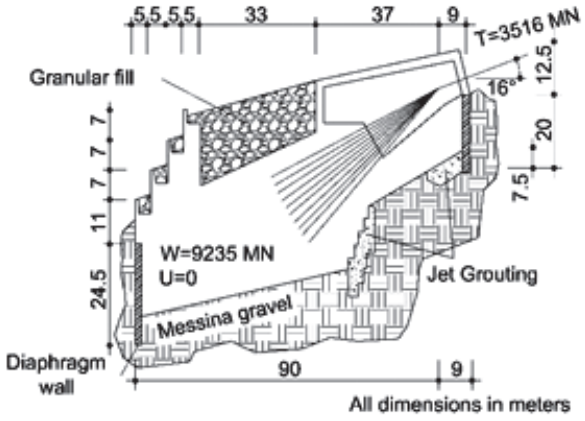

Fig. 21. Anchor block on Sicilian shore

4. Special Geotechnical Investigations for the final design

Additional geotechnical tests were carried out for the final design but actually they cannot be published. However, a trial investigation was conducted in preparation of the next geotechnical campaign [Lo Presti et al. 2006]. Some details are given in the present section.

Fig. 22 shows the location of the Terrarossa site. Due to budget restraint, it was decided to retrieve frozen samples from a depth of 2.0 m below the ground level down to 6.0 m. For this purpose guide pipes have been preliminarily installed in agreement with the usual practice [Hatanaka et al. 1988, Goto et al. 1992]. More specifically five steel pipes about 2.0 m long connected by two flanges at the ends have been installed in a pre-drilled hole of about 1.5 m in diameter. After the installation of the guide pipes and the check of their verticality, the pre-drilled hole was filled with concrete. This operation was accomplished three weeks before the starting of the in situ freezing. The central pipe was used to install the double — tube freezing pipe, necessary for the circulation of the LN_2. The freezing pipe was extended down to 8.0 m below the ground level. The shallower portion of the freezing pipe (about 2.0 m) was thermally isolated. Three pipes were necessary to guide the double core barrel; the fourth pipe was used to install a number of thermocouples. This pipe was inclined of about 4° to locate the thermocouples at increasing radial distances with depth.

Figs. 23 and 24 show respectively a picture of the guide-pipes and the plant of the guide-pipes at ground level.

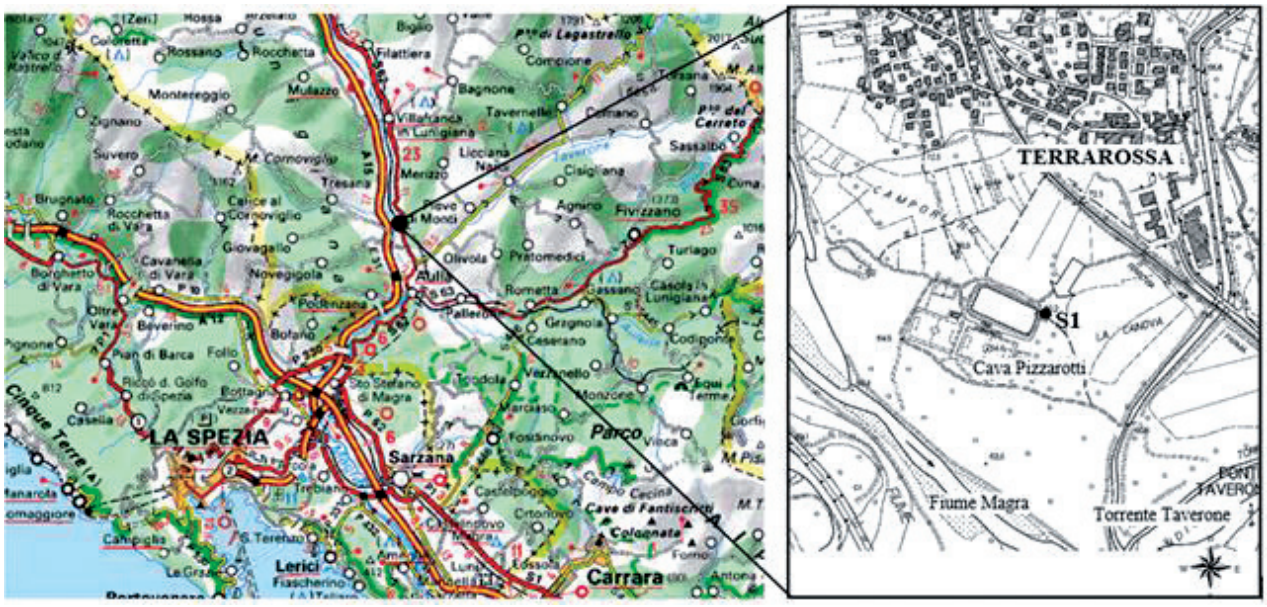

Fig. 22. Site location

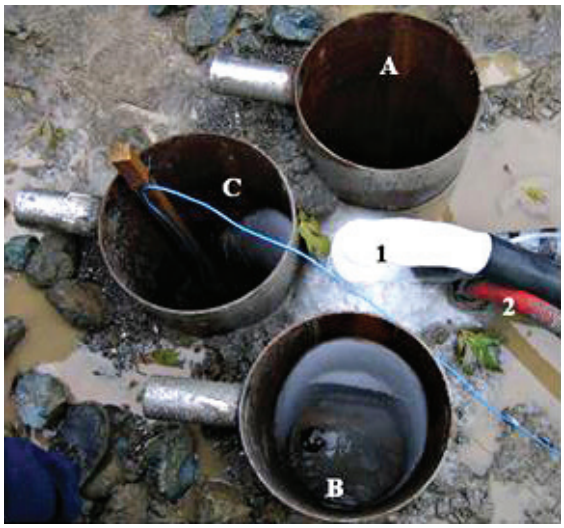

Fig. 23. Guide pipes picture

Unlike the usual method [Goto et al 1992] only three frozen samples were retrieved at each depth, because of budget restraint. As for the temperature control, 7 thermocouples were installed. The shallower thermocouple was located at 2.0 m depth with a radial distance of 0.35 m.

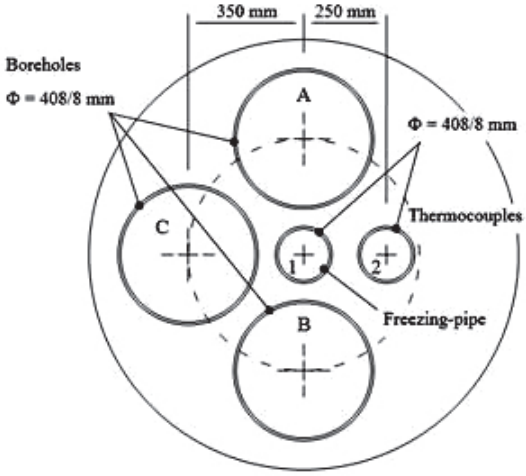

Fig. 24. Guide pipes plant

The other thermocouples were installed at increasing depth and radial distances as precisely shown in Fig. 25.

Figs. 26 and 27 show respectively the temperature monitoring and the LN_2 consumption with time. Thermocouples were fixed onto a PVC tube, which was inserted into the inclined guide-pipe and inclined hole. The space between the PVC tube and the hole was filled with mortar pumped from the bottom. Initial high temperatures are due to the chemical reactions of mortar. As for the temperature, it is clear that a target value of about −10 °C was reached in most of the target zone after about 5 days (120 hours), while on the other hand the deeper and more external thermocouples never reached temperature below zero °C. It is supposed that the frozen zone had a radius of no more than 0.70 m. Moreover, temperature into the soil rapidly increases above zero °C at short distance from the frozen front, showing a very high gradient.

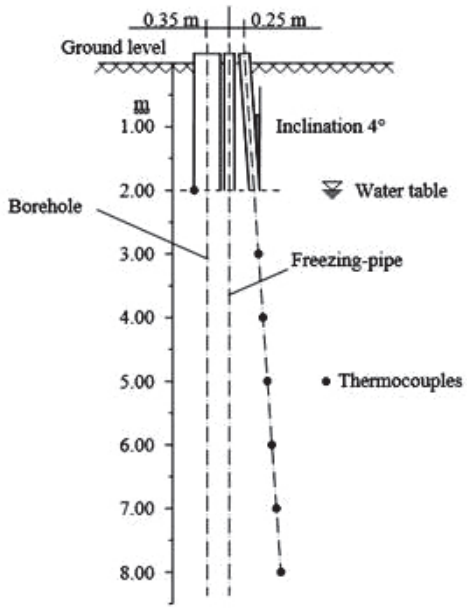

Fig. 25. Thermocouples location

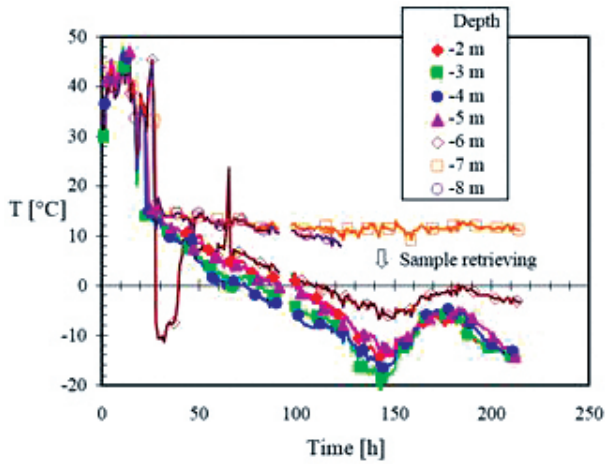

Fig. 26. Freezing monitoring at Licciana Nardi: temperatures

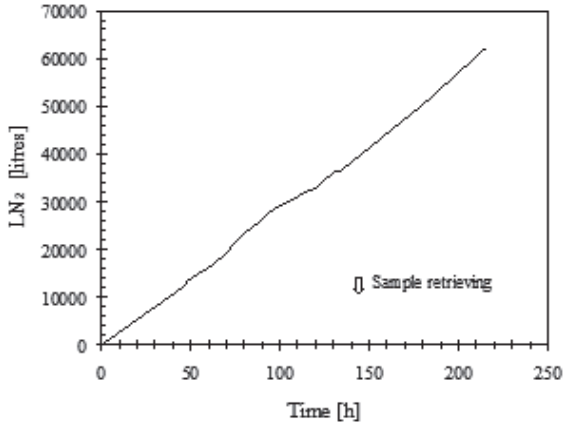

Fig. 27. Freezing monitoring at Licciana Nardi: consumption

Consumptions are expressed in litres. In order to freeze the soil about 290 kN of LN_2 were necessary. The total consumption of LN_2 was of about 500 kN.

Fig. 28 shows a retrieved sample and Fig. 29 shows the individual geotechnical drilling operations and the full set of samples retrieved. Samples have a diameter of 298.0 mm and height of approximately 600.0 mm.

Fig. 28. Sample A3, depth 4.10–1.70m

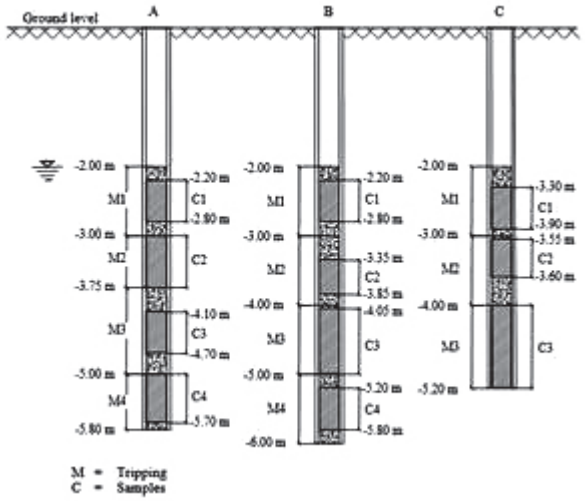

Fig. 29. Retrieved samples

5. Laboratory testing

The triaxial cell was designed and realized in the framework of a research contract between ENEL–CRIS of Milan (which is the owner of the cell) and the Politecnico di Torino [Lo Presti et al. 1997], and it was preliminary used in the framework of such a research contract [Lo Presti et al. 1997, Pietrobono 1998]. The cell has been improved in recent years [Fiorio 2003, Rinolfi 2005, Lo Presti et al. 2004].

The main characteristics of the triaxial cell structure are similar to those accepted for advanced equipments [Tatsuoka 1988, Lo Presti et al. 1994] and can be summarised as follows:

- the structure is very stiff (low compliance);
- the tie rods are inside the pressure cell;
- the loading ram is fixed to the top cap (any type of stress-path is possible);
- the loading ram is virtually frictionless, which is a basic requirement for an accurate control of the applied stress or strain [Tatsuoka, 1991];
- the correct alignment between loading ram, top cap and specimen is guaranteed by the high accuracy in the cell construction and limited tolerance required;
- the weight of the loading ram and top cap is counter-weighted;
- because of the size and weight of the cell an appropriate system to move it is required.

Fig. 30. Triaxial cell

The loading system consists of a reaction frame and a hydraulic piston with a capacity of 1000 kN and a maximum stroke of ±100 mm. Hydraulic piston and loading ram are connected by a spherical bearings. The piston is controlled by an MTS System and it is possible to operate in terms of displacement, pressure or force control. As regards specimens having a diameter $D = 300$ mm and height $H = 600$ mm the minimum strain and stress that can be controlled are $g_a = 1.7*10–3\,\%$ and $\sigma_a = 0.3$ kPa.

The minimum and maximum displacement rates are respectively 10^{-9} m/s and 400 m/s. When using sinusoidal waveform it is possible to operate in the frequency interval from 0.001 Hz to 80 Hz.

Cell and back pressures are regulated by means of PC controlled electro valves having a resolution of 0.1 kPa.

Data acquisition and stress or strain path control are accomplished by means of a PC equipped with a 16 bit A/D converter (333000 samples/s).

Control software has been developed by LabVIEW (National Instruments).

- During a test the following stresses and strains are measured:
- External axial strain by means of an LVDT (stroke ±100 mm, resolution < 0.01 mm);
- Local axial strain by means of three LDT [Goto et al. 1991], located along the lateral surface of the specimen at 120°. (stroke 20 mm, resolution < 0.002 mm)
- Axial load by means of an internal load cell (stroke = ±200 kN, resolution < 0.02 kN);
- Cell and pore pressure by means of pressure transducers (maximum capacity 10 bar);
- Measurements of volume change have been done using a low-compliance burette system equipped with a differential pressure transducer in agreement with the suggestion by Pradhan et al. (1986). The smallest accurate measurement of volumetric strain is 0.0018 %.

5.1. Procedures for specimen reconstitution

Each specimen was reconstituted in 20 layers, each of wich was formed by hand pouring the soil in a mould levelling the upper surface by hand. No compaction has been used and generally a density slightly lower than that of undisturbed samples was obtained. In order to guarantee a high saturation degree, the water level inside the forming sample was progressively raised during the reconstitution process until the water height was coincident with the current specimen height.

6. Experimental results

6.1. Soil stiffness and damping ratio

Triaxial tests were performed on isotropically consolidated specimens. Table 6 summarizes the test conditions at the end of consolidation.

Table 6

Test condition (Undrained Triaxial Monotonic and Cyclic compression Loading tests)

Frozen samples			
	C2	A3	B4
z (m)	3.05–3.60	4.10–4.70	5.20–5.80
e (-)	0.271	0.246	0.302
σ'_c (kPa)	60.5	69	82.7
reconstituted samples			
	C2	A3	B4
z (m)	3.05–3.60	4.10–4.70	5.20–5.80
e (-)	0.373	0.302	0.488
σ'_c (kPa)	46.2	47.6	47.2

One-way cyclic compression loading triaxial tests were performed in undrained condition under strain control using a triangular waveform with strain rate ranging from: $\dot{\varepsilon}_a = 0.2\,\%/\text{min}$ to $\dot{\varepsilon}_a = 0.5\,\%/\text{min}$.

The single amplitude cyclic strain levels applied during each test were tentatively: 0.001, 0.002, 0.005, 0.01, 0.02, 0.05, 0.1 %, and for each step 19 loading cycles were applied. Figures 31, 32 and 33 show typical test results for a given loading step. It is possible to observe a typical cyclic strain softening behaviour with a progressive stiffness reduction and progressive reduction of the loop area, which is rather unusual if compared with available data in the technical literature. Equivalent Young's modulus E_{eq} and damping ratio D have been determined in the following way:

$$E_{eq} = \frac{q_{SA}}{(\varepsilon_a)_{SA}} \tag{10}$$

where q_{SA} and $(\varepsilon_a)_{SA}$ are single amplitude, respectively, of q and ε_a during cyclic loading.

Damping ratio was computed as:

$$D = \frac{\Delta W}{4\pi W} \tag{11}$$

where ΔW is the area enclosed by the unloading-reloading loop and represents the total energy loss during the cycle and W is the elastic stored energy.

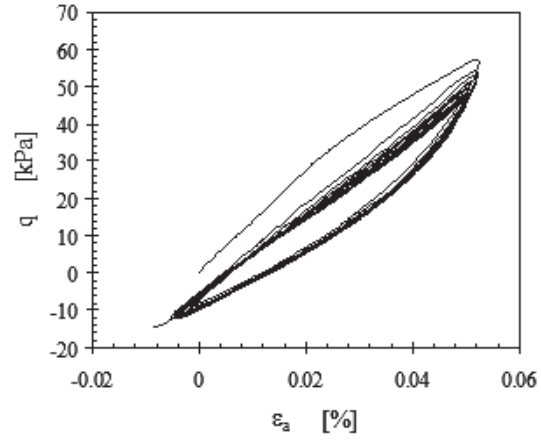

Fig. 31. Typical results from strain controlled cyclic tests

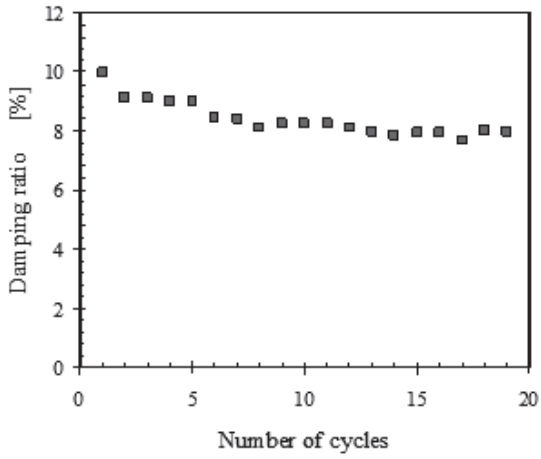

Fig. 32. Typical results from strain controlled cyclic tests

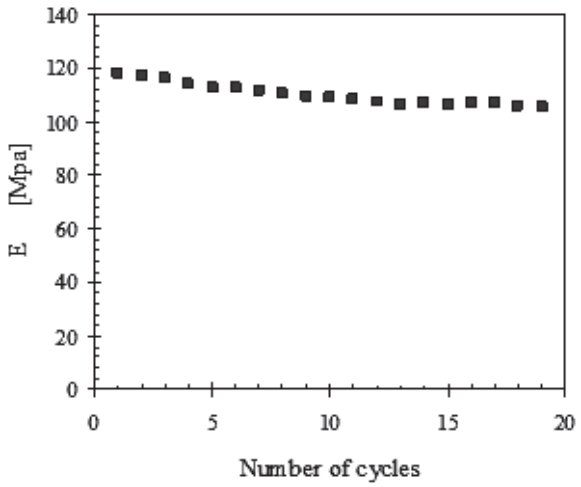

Fig. 33. Typical results from strain controlled cyclic tests

In each test, after the highest strain level has been imposed to the specimen, the drainage was opened and the specimen was let in drained conditions for, at least, 24 hours. After such a rest period, the specimen was subjected to monotonic loading triaxial compression in undrained conditions under constant rate of strain $\dot{\varepsilon} = 0.5\,\%/\text{min}$. Figs. 34 and 35 show a typical test result.

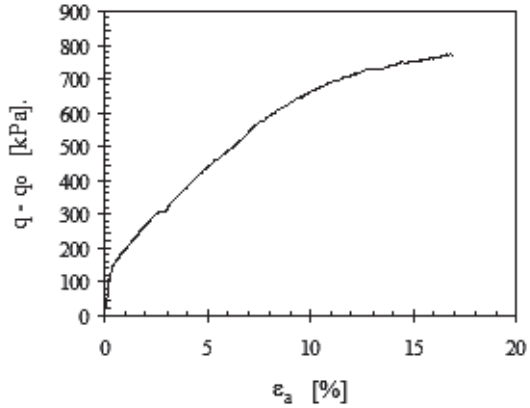

Fig. 34. Typical results from strain controlled monotonic loading test

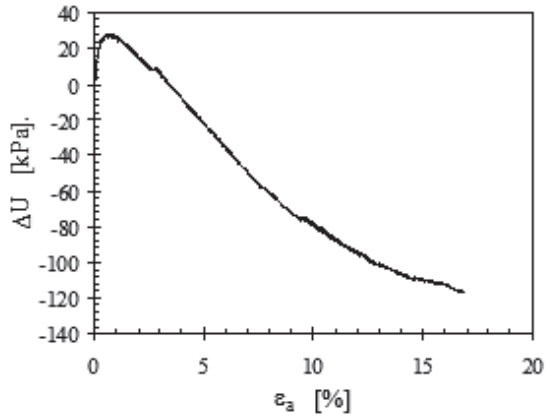

Fig. 35. Typical results from strain controlled monotonic loading test

The secant stiffness E from monotonic loading triaxial tests was determined in the following way:

$$E = \frac{(q - q_o)}{\varepsilon_a} \qquad (12)$$

where q_o is the value of deviator stress from which the secant stiffness is defined (ε_a). In other words q_o is the value of deviator stress at the end of the (isotropic) consolidation and therefore is essentially equal to zero.

The same types of tests (cyclic and monotonic) were repeated on reconstituted samples. Table 6 summarizes test conditions also for the reconstituted samples. Table 6 shows differences in terms of e and σ'_c between undisturbed and reconstituted samples. Small differences of void ratio are due to intrinsic and unavoidable limitations of the adopted reconstitution method.

Fig. 36 compares the secant stiffness obtained from undrained monotonic loading triaxial compression tests and those inferred from undrained cyclic loading triaxial compression tests.

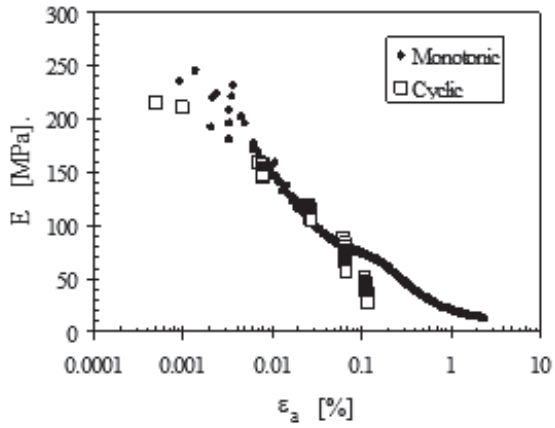

Fig. 36. Comparison between undrained monotonic and cyclic loading triaxial compression tests — Young's modulus

The results shown in Fig. 36 can be explained in the following way:

- stiffness from undrained cyclic and monotonic loading tests is almost the same, up to strain values of 0.01 %. For larger strains the stiffness from cyclic loading tests is smaller than that observed in monotonic loading tests, especially after the application of a certain number of loading cycles (N). This is probably due to the different mechanism of pore pressure accumulation. In cyclic tests the pore pressure continuously increases, whilst in monotonic tests dilatancy can produce reduced or even negative pore pressure. Therefore it is believed that the pore pressure accumulated in cyclic tests at large strains is higher than that observed in monotonic loading tests (see Fig. 37). external axial strain

measurements largely underestimate the soil stiffness in comparison to local measurements up to a strain level of about 0.1 %.

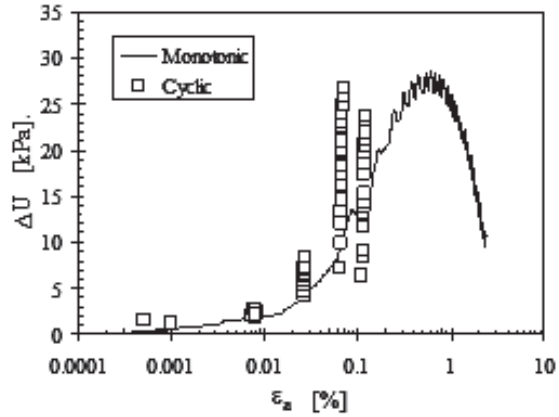

Fig. 37. Comparison between undrained monotonic and cyclic loading triaxial compression tests — pore pressure

Figs. 36 and 37 compare the results obtained on undisturbed and reconstituted samples. More specifically Fig. 38 compares the stiffness E, as obtained from cyclic loading tests, of undisturbed and reconstituted samples. Soil stiffness has been divided by the initial or small strain modulus E_o. Fig. 39 compares the damping ratio. Both Figures indicate that the normalized stiffness and damping ratio of undisturbed and reconstituted samples are very similar. As for the stiffness, this result is in agreement with to data shown by several researchers [Goto et al. 1987, 1992, 1994, Hatanaka et al. 1988, Hatanaka and Uchida 1995, Yasuda et al. 1994]. Even data by Kokusho and Tanaka (1994) do not show very relevant differences between the normalized stiffness of undisturbed and reconstituted samples. As for the damping ratio, the already mentioned works show contradictory indications.

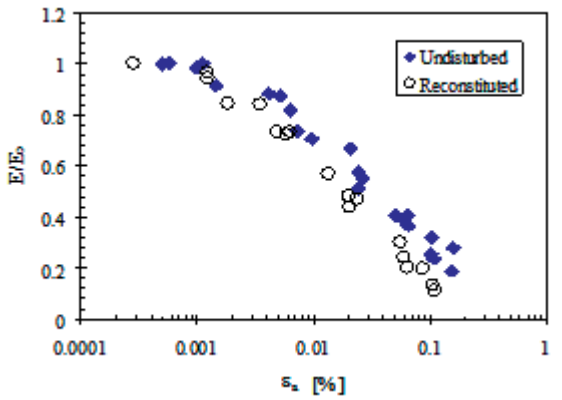

Fig. 38. Results of cyclic loading triaxial compression test performed on undisturbed and reconstituted gravel samples — normalized stiffness

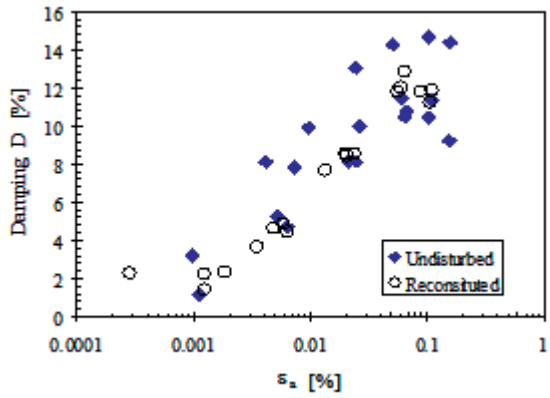

Fig. 39. Results of cyclic loading triaxial compression test performed on undisturbed and reconstituted gravel samples: damping ratio

The small strain stiffness of undisturbed samples resulted to be up to 20 % greater than that of reconstituted samples, but in most cases Eo. of undisturbed samples was very close to that of reconstituted samples tested under same conditions (void ratio e, consolidation pressure σ'_c).

To account for the differences in terms of e and σ'_c, data have been normalized according to the following dimensionless equation [Lo Presti 1989]:

$$E_o = S \cdot e^{-1,1} \cdot \sigma'^{0.5}_c \cdot p_a^{0.5} \qquad (13)$$

where: p_a = atmospheric pressure expressed in the same unit as stiffness and consolidation pressure and S = soil constant, ranging between 400 and 800. Data available in literature indicate that the small strain stiffness of undisturbed samples from recent Holocene deposits is on average 30 % greater than that measured in the case of reconstituted samples [Goto et al. 1987, 1992, 1994, Hatanaka et al. 1988, Kokusho and Tanaka 1994, Yasuda et al. 1994, Hatanaka and Uchida 1995].

6.2. Cyclic undrained strength

Liquefaction tests were performed on isotropically consolidated specimens. More specifically, one way cyclic compression loading triaxial tests were performed in undrained condition under stress control. Table 7 summarizes test conditions at the end of consolidation.

Table 7

Test condition (Liquefaction tests)

Frozen samples			
	A1	C1	B3
z (m)	2.20–2.80	2.30–2.90	4.05–4.70
e (-)	0.29	0.333	0.332
σ'_c (kPa)	47.6	45.8	54.1
reconstituted samples			
	A1	C1	B3
z (m)	–	2.30–2.90	4.05–4.70
e (-)	–	0.388	0.373
σ'_c (kPa)	–	42.6	46.2

The deviator stress σ_d, which was applied during undrained shearing, is also indicated in Table 5 and, in brackets, the cyclic stress ratio (CSR= $\sigma_d/2\sigma'_c$). Figs. 40 and 41 show typical test results.

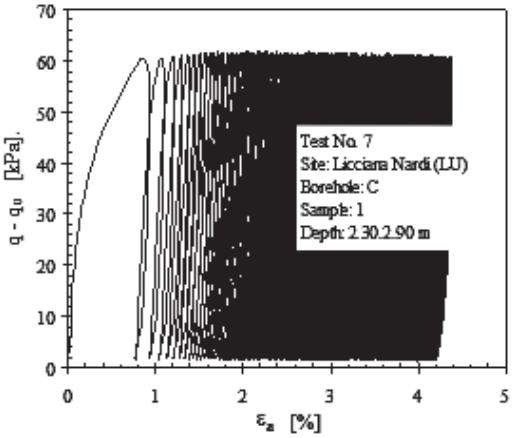

Fig. 40. Undrained cyclic compression loading triaxial test-loading curve

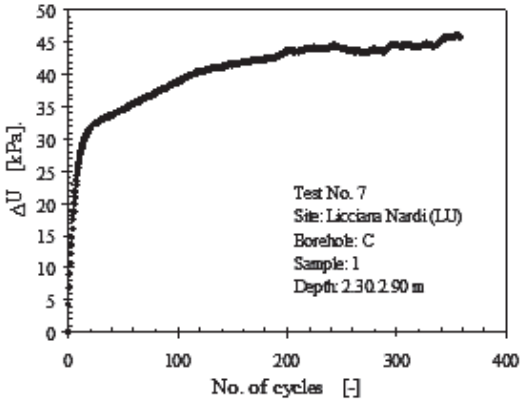

Fig. 41. Undrained cyclic compression loading triaxial test: pore pressure

Liquefaction tests were repeated on reconstituted samples but the results will be not discussed in this paper.

Fig. 42 compares the CSR, obtained in this research on undisturbed samples, to those obtained by Kokusho and Tanaka (1994) on gravely undisturbed samples.

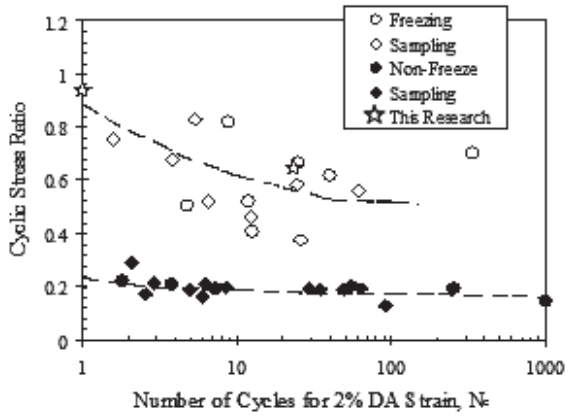

Fig. 42. Comparison of CSR obtained in this research on undistrurbed samples

The CSR was defined as the normalized deviator stress, which causes 2 % single amplitude axial strain in a given number of cycles. This condition (for the tests performed in this research) coincides with a pore pressure ratio equal to 1.0 (zero-effective consolidation pressure). It is worthwhile to remark that the agreement with the data by Kokusho and Tanaka (1994) is a coincidence and the only possible conclusion is that the liquefaction strength of undisturbed samples is much larger than that usually obtained from reconstituted samples. It is also important to notice that only two of the three tested samples liquefied.

Table 8 summarizes the liquefaction test results. More specifically, the table shows:

- relative density of the frozen samples;
- effective consolidation pressure (σ_c);
- applied deviator stress (σ_d) and, in brackets, the CSR;
- number of loading cycles causing liquefaction;
- gravel (GC), sand (SC) and fine contents (FC).

Table 8

Liquefaction tests results

D_r (%)	σ_c (kPa)	σ_d (CSR) (kPa)	N	GC (%)	SC (%)	FC (%)
70	47.6	95 (0.98)	1	81	14	5
87	45.8	60 (0.66)	20	47	31	22
37	54.1	80 (0.74)	–	80	19	1

It is worthwhile to remark that the liquefaction condition appears to be more regulated by compositional factors than global relative density. It should be stressed that the samples that liquefied exhibit a quite important percentage of medium to-fine-sand, whilst the sample that did not liquefy consists of gravel and coarse- to-medium sand.

Acknowledgement

Prof. M. Jamiolkowski (Technical University of Turin) was the principal geotechnical consultant of SdM for the preliminary and final design. Prof. E. Faccioli (Technical University of Milan) was the principal consultant for the definition of the design earthquake. The first Author of this paper has been working as consultant of Parsons Ltd. for the design of special geotechnical investigations.

References

1. Jamiolkowski M. & Lo Presti D. Geotechnical Characterization of Holocene and Pleistocene Messina sand and gravel deposits. *Invited Lecture International Workshop on Characterization and Engineering Properties of Natural Soils* (National University of Singapore, Dec. 2002), Balkema, 2003, vol. 2, pp. 1087–1120.

2. Lo Presti D., Pallara O., Froio F., Rinolfi A., Jamiolkowski M. Stress-strain-strength behaviour of undisturbed and reconstituted gravelly soil samples. *Rivista Italiana di Geotecnica Anno XL*, 2006, no. 1, pp. 9–27.